Remote Sensing of Environment 198 (2017) 460–470

Contents lists available at ScienceDirect

Remote Sensing of Environment

journal homepage: www.elsevier.com/locate/rse

L-band vegetation optical depth and effective scattering albedo estimation from SMAP

Alexandra G. Konings [a], Maria Piles [b], Narendra Das [c], Dara Entekhabi [d,*]

[a] Department of Earth System Science, Stanford University, Stanford, CA 94305, United States
[b] Image Processing Lab (IPL), Universitat de València, 46980, Valencia, Spain
[c] Jet Propulsion Laboratory, California Institute of Technology, Pasadena, CA 91109, United States
[d] Ralph M. Parsons Laboratory for Environmental Science and Engineering, 48-216C, Massachusetts Institute of Technology, Cambridge, MA 02139, United States

ARTICLE INFO

Article history:
Received 24 March 2017
Received in revised form 2 June 2017
Accepted 28 June 2017
Available online xxxx

Keywords:
Vegetation optical depth
Effective scattering albedo
L-band radiometry

ABSTRACT

Over land the vegetation canopy affects the microwave brightness temperature by emission, scattering and attenuation of surface soil emission. Attenuation, as represented by vegetation optical depth (VOD), is a potentially useful ecological indicator. The NASA Soil Moisture Active Passive (SMAP) mission carries significant potential for VOD estimates because of its radio frequency interference mitigation efforts and because the L-band signal penetrates deeper into the vegetation canopy than the higher frequency bands used for many previous VOD retrievals. In this study, we apply the multi-temporal dual-channel retrieval algorithm (MT-DCA) to derive global VOD, soil moisture, and effective scattering albedo estimates from SMAP Backus-Gilbert enhanced brightness temperatures posted on a 9 km grid and with three day revisit time. SMAP VOD values from the MT-DCA follow expected global distributions and are shown to be highly correlated with canopy height. They are also broadly similar in magnitude (though not always in seasonal amplitude) to European Space Agency Soil Moisture and Ocean Salinity (SMOS) VOD. The SMOS VOD values are based on angular brightness temperature information while the SMAP measurements are at a constant incidence angle, requiring an alternate approach to VOD retrieval presented in this study.

Globally, albedo values tend to be high over regions with heterogeneous land cover types. The estimated effective scattering albedo values are generally higher than those used in previous soil moisture estimation algorithms and linked to biome classifications. MT-DCA retrievals of soil moisture show only small random differences with soil moisture retrievals from the Baseline SMAP algorithm, which uses a prior estimate of VOD based on land cover and optical data. However, significant biases exist between the two datasets. The soil moisture biases follow the pattern of differences between the MT-DCA retrieved and Baseline-assigned VOD values.

1. Introduction

Microwave vegetation optical depth (VOD) is proportional to the vegetation water content (VWC) of the above-ground canopy biomass (Wigneron et al., 2017; Ulaby and Long, 2014; Jackson and Schmugge, 1991) and constitutes a potentially useful indicator of the vegetation state. Datasets of VOD retrievals from high microwave frequencies such as K-band, X-band or C-band (Jones et al., 2010; Liu et al., 2011) have previously been used for a variety of carbon cycle studies. These VOD data have been used for understanding vegetation seasonality (Guan et al., 2013, 2014), North American and African growing season length (Jones et al., 2012; Barichivich et al., 2013; Vrieling et al., 2013), long term trends in woody vegetation (Andela et al., 2013; Liu et al., 2015; Tian et al., 2016a), and the effects of overgrazing in Mongolia (Liu et al., 2013), etc. Because VWC and VOD are also sensitive to vegetation water stress, diurnal variations in VOD can also be used to understand spatial variations in ecosystem-scale drought response (Konings and Gentine, 2017) and how this affects the relative sensitivity of photosynthesis to precipitation and vapor pressure deficit (Konings et al., 2017).

The datasets used in the above studies and other studies of VOD dynamics most commonly rely on one of two datasets of VOD retrieved from the Japanese Advanced Microwave Scanning Radiometer (AMSR-E) using two different retrieval algorithms and frequencies. The University of Montana (UMT) approach (Jones et al., 2010, 2011) retrieves VOD from the X-band and K-band frequencies (23 GHz and 18.7 GHz) of AMSR-E, by first determining the open water fraction of the pixel, cloud liquid water content, and surface temperature and then determining an effective land surface emissivity at X-band. At this frequency, penetration into the soil (and thus the dependence on soil moisture) is limited, and therefore the VOD is retrieved assuming a given albedo and

* Corresponding author.
E-mail address: darae@mit.edu (D. Entekhabi).

http://dx.doi.org/10.1016/j.rse.2017.06.037
0034-4257/

soil reflectivity. By contrast, the Land Parameter Retrieval Model (LPRM) approach is applied to either the C-band (6.9 GHz) or X-band (10.7 GHz) frequency channels of AMSR-E. Since these are lower frequencies, they are less sensitive to cloud liquid water content and more sensitive to soil moisture (and to deeper canopy layers) (Ulaby and Long, 2014). The LPRM approach (Meesters et al., 2005; Owe et al., 2008) (cf. references therein to LPRM heritage) therefore neglects atmospheric effects and retrieves soil moisture and vegetation optical depth from snapshots of dual-polarized observations simultaneously. The LPRM approach has also been applied to other satellites (Liu et al., 2011; Van der Schalie et al., 2015).

These AMSR-E VOD retrievals have several drawbacks. High frequency measurements outside research-protected frequency bands are sensitive to radio frequency interference (RFI) (e.g., tracking radar and telecommunications) (Njoku et al., 2005) and cloud liquid water effects on the temperature estimates. In addition, depending on location, AMSR-E VOD may primarily be sensitive to the top of the vegetation, since at these frequencies the signal is more sensitive to leaf orientation (Matzler, 1994). If used for hydraulic stress applications, considering only the top of the canopy neglects the significant variability in stress that is possible across canopy height (Hellkvist et al., 1974). Furthermore, both AMSR-E approaches rely on snapshots of multi-polarization brightness temperatures. As discussed further below, this approach may lead to compensating errors (Konings et al., 2011, 2015). Last but not least, both algorithms assume a prior, globally constant assumption on the value of the scattering albedo, which affects the retrieved VOD values (though note Du et al. (2015) have recently made improvements by incorporating a spatially variable albedo into the UMT approach).

Alternatively, a new generation of L-band radiometers has been launched over the last decade with the potential to measure VOD: the European Space Agency SMOS (Kerr et al., 2010), the joint National Aeronautics and Space Administration (NASA)/Argentinian Aquarius-SAC/D (Le Vine et al., 2010), and the NASA SMAP (Entekhabi et al., 2014) missions. The L-band microwave part of the spectrum contains spectral regions that are reserved for scientific research and therefore should have less RFI. It is also more sensitive to deeper layers of vegetation canopy, is insensitive to cloud liquid water, and is sensitive to deeper soil moisture layers.

SMOS was the first mission dedicated to soil moisture and ocean salinity remote sensing. The SMOS antenna is six meters in scale and through aperture synthesis provides images of the surface across a 1000 km wide swath at about 40 km resolution as it orbits the Earth. The wide swath results in irregular revisit times depending on latitude. Most regions across the globe are sampled at least every two to three days. The SMOS radiometer produces estimates of land L-band emission at a variety of angles. Therefore it has the potential to use angular information to infer properties of the soil and vegetation simultaneously.

In recent years SMOS global L-band observations have been used to derive a unique data set on lower microwave frequency VOD. The SMOS VOD retrievals are formed using the multi-angular and polarimetric information in the brightness temperatures. The SMOS measurements are used to simultaneously invert VOD and surface soil moisture. The algorithm has evolved over time (see Wigneron et al., 2017 for review). Most notably and in recent years, Vittucci et al. (2016) has advanced the capability to retrieve L-band SMOS VOD over forested landscapes. The SMOS VOD fields have been studied extensively. Grant et al. (2016) compare the SMOS VOD to AMSR-E VOD. They also consider global fields of optically-based vegetation indices. They find that the spatial patterns and dynamics of the two microwave-based vegetation parameters are similar in general but clear distinctions are also evident in particular regions. The SMOS VOD has higher correlation with the AMSR-E VOD than with optical vegetation indices. The higher microwave frequency AMSR-E VOD, in turn, is more correlated with the optical indices that the SMOS VOD. These results suggest the lower frequencies are more representative of the canopy volume than the higher frequencies, as expected. Lawrence et al. (2014) also compared (a previous version of) SMOS VOD with optical vegetation indices, finding an interesting difference in the timing of the annual peak in the two time-series over major cropped zones. The SMOS VOD time-series peak about 19 days later than optical vegetation indices, suggesting sensitivity of VOD to crop canopy attributes not observable using optically-based indices. In another study Patton and Hornbuckle (2013) find that the change in SMOS VOD is correlated with patterns of crop yield in a more focused sub-region of Iowa croplands. Parrens et al. (2016) combine the vegetation and roughness effects into a single parameter and estimate it using SMOS brightness temperatures at global scale. They then use optical leaf area index ancillary information to separate the roughness and vegetation factors. The estimate surface roughness parameter is analyzed globally.

Another version of VOD retrievals using SMOS L-band measurements has recently become available (Fernandez-Moran et al., 2017). The SMOS-INRA-CESBIO or SMOS-IC version is designed to be as independent of ancillary information as possible (INRA is Institut National de la Recherche Agronomique and CESBIO is Centre d'Etudes Spatiales de la BIOsphère). It treats individual data granules in SMOS data products as homogeneous in land use and defines different values of effective scattering albedo and surface roughness than the earlier SMOS products. Fernandez-Moran et al. (2017) report that the VOD retrievals between the earlier and SMOS-IC versions have comparable spatial mean maps and seasonal dynamics, with the newer data set having slightly lower values.

In 2011, NASA in collaboration with the Argentinian space agency launched and operated the Aquarius instrument which also included an L-band radiometer but was accompanied by an L-band scatterometer that enhanced the capability to monitor global ocean salinity (Le Vine et al., 2010). The Aquarius instrument made pushbroom measurements of the Earth surface with a real aperture (reflector) antenna of 2.5 m in diameter. With similar orbit but smaller antenna size than SMOS, the Aquarius resolution was significantly lower: its spatial resolution was about 100 km with a 7-day revisit time. Aquarius made 3.5 years of active-passive measurements ending in early 2015 due to a failure in the electronics supplying power to the observatory attitude control system.

During the last decade or so, NASA designed and implemented the L-band SMAP mission (Entekhabi et al., 2014), which was launched in January 2015. It uses a real aperture antenna that has the same dimension and hence half power (−3 dB antenna gain) sensing resolution as SMOS. SMAP also carried a radar capable of synthetic aperture processing and close to 3 km resolution for most of the instrument field-of-view. However, after two months of operations its radar ceased to make further measurements due to a hardware anomaly. The SMAP antenna is a light-weight mesh reflector that deployed from a stowed configuration to allow real aperture sensing. It is rotated to make a conical scan over a 1000 km swath. With similar orbits, SMAP and SMOS have nearly the same revisit rate. The SMAP instrument also implemented a number of hardware and software measures to detect and where possible mitigate anthropogenic RFI, which is prevalent around the globe despite SMAP operating in an internationally protected band (Mohammed et al., 2016).

The multi-angular retrieval approach used by SMOS is not possible for SMAP, which only collects single incidence-angle measurements. As a result, there are essentially two sets of possible observations at two polarizations and three unknowns: soil moisture, VOD, and the effective scattering albedo. In order to retrieve soil moisture, the Baseline SMAP algorithm assumes a prior value of the scattering albedo based on land cover and an estimate of VOD based on Normalized Difference Vegetation Index (NDVI) climatology and land cover type (Chan, 2013b; Kim, 2013). A roughness height parameter is also assumed based on land cover. These parameters are then used in a so-called single-channel algorithm to find the soil moisture value that best matches the observed V-polarized brightness temperature. Although VOD and NDVI show some (intermediate) correlation across spatial and temporal scales (Grant et al., 2016)they are fundamental measures of different

vegetation properties (vegetation water content and canopy greenness, respectively), so that a VOD prediction based on NDVI may incur significant errors. Derivation of an alternative approach for estimating and accounting for VOD from SMAP measurements may thus be useful both for ecological studies and to improve SMAP soil moisture retrievals.

However, tests by the SMAP team of a dual-channel snapshot algorithm that uses both the H-polarized and V-polarized brightness temperatures to retrieve VOD and soil moisture simultaneously have concluded that this approach actually leads to higher soil moisture retrieval errors, despite relying on additional information (Crow et al., 2005; O'Neill et al., 2015). This is consistent with previous simulation experiments that showed that a snapshot dual-channel algorithm can lead to large but compensating (i.e., opposite) errors in VOD and soil moisture that can nevertheless lead to a close match to observations (Konings et al., 2011). It should be noted that the snapshot dual-channel algorithm does outperform single-channel algorithms in some specific cases of ground-truth validation studies (see Table V in Chan et al. (2016)). Interestingly, the improved performance is mostly over regions with agricultural land use where crop phenology changes rapidly and with different timing each year.

The dual-channel retrieval problem is under-determined and poses challenges due to the close correlation between observed horizontal and vertical brightness temperatures. Konings et al. (2015) introduced the Degrees of Information (DoI) to argue that the two sets of observations do not allow for accurate retrieval of two independent variables by themselves. Attempting to do so leads to a retrieval cost function with a multitude of local minima and a flat 'valley' of low cost function values, as demonstrated in Konings et al. (2016). Thus, only small amounts of observation noise or imperfections in the cost function minimization will lead to erroneous retrievals, including high-frequency noise due to jumps between local minima (Konings et al., 2016). The DoI of observations can be used to ensure no more parameters are retrieved than the information content in the observations allows.

Konings et al. (2016) introduced the multi-temporal dual channel algorithm (MT-DCA), which assumes that VOD changes more slowly than soil moisture and can be assumed to be almost constant between every two consecutive overpasses. The MT-DCA then adds an additional constraint to the retrieval problem by using a moving window of two consecutive overpasses at a given time of day, and jointly retrieving a single value of VOD and two values of the soil dielectric constant or soil moisture. In addition, the time series approach allows for the retrieval of a single temporally constant value of the scattering albedo per pixel. The MT-DCA was developed using Aquarius data (Konings et al., 2016), but it is unclear to what degree the low 7-day Aquarius revisit time, as well as the fact that the Aquarius orbit is not perfectly repeating (McColl et al., 2014b; Piles et al., 2015) reduces the validity of the moving window VOD assumption. Furthermore, the low (~100 km) spatial resolution of the Aquarius data is prohibitively large for in situ validation of the soil moisture retrievals.

In this paper, we apply the MT-DCA to the first full year of SMAP observations.

Section 2 summarizes the algorithm details and introduces the specific datasets used. In Section 3, the resulting VOD and scattering albedo retrievals are compared to each other, and correspondence of multi-temporal VOD with SMOS-derived VOD and lidar canopy height is analyzed. Additionally, the impact of accounting for spatial and temporal variations in VOD and albedo through the MT-DCA approach on soil moisture retrieval is discussed by comparing the MT-DCA retrievals to those from the Baseline SMAP single channel algorithm.

2. Methods

2.1. Summary of MT-DCA

The MT-DCA is introduced in Konings et al. (2016), but summarized here for convenience. Like most passive microwave algorithms for land surface retrievals, it is based on the zeroth-order solution to the radiative transfer equations known as the tau-omega model (Kerr and Njoku, 1990):

$$T_{B_p} = T_{B_p}^{soil} + T_{B_p}^{veg} = T_{soil}\left(1-r_p^{rough}\right)\gamma + T_{veg}(1-\gamma)(1-\omega) \times \left(1+\gamma r_p^{rough}\right), \quad (1)$$

where $T_{B_p}{}^{soil}$ and $T_{B_p}{}^{veg}$ are the soil and vegetation contributions to the p-polarized observed brightness temperature T_{B_p}. The rough soil surface reflectivity is r_p^{rough} at p-polarization. The T_{soil} and $T_{vegetation}$ are the soil and vegetation temperatures, which are assumed to be equal during the 6:00 AM SMAP descending overpass. The vegetation layer attenuates the soil contribution in an amount dependent on its transmissivity $\gamma = \exp(-\mathrm{VOD}\cdot\sec\theta)$, where θ is the observation angle (see Wigneron et al. (2017) Section 4 for a comprehensive discussion of vegetation effects and treatment in emission models). The effective scattering albedo is the dimensionless parameter ω. It is dependent on the structure and composition of the vegetation and (as we will show later on this paper) to landscape heterogeneity. It has previously been shown that a slightly lower effective value of ω can be used to partially account for higher-order scattering without changing the model formulation (Kurum et al., 2012; Kurum, 2013), so that the retrieved albedo values can be interpreted as effective values. Consistent with other passive microwave retrievals, we assume that the vegetation parameters are polarization-independent for the sake of parsimony. This assumption also reduces the number of parameters that need to be estimated and allows for likely more robust but effective parameter retrievals. This assumption may not hold over e.g. agricultural fields and certain managed forests where the field of view has a regular structure. However, given the 40 km size of each antenna footprint, the overall scene is likely to be have random geometry and lack the consistent structure that can cause distinct polarization.

As discussed above, the problem of retrieving soil moisture s (which influences r_p^{Rough}), VOD, ω, and possibly a roughness parameter all from a set of single incidence angle, dual-polarized observations is underdetermined. The MT-DCA uses a moving window to combine retrievals from two consecutive overpasses, assuming VOD is constant over those overpasses. Thus, it is the minimum of the cost function,

$$\min_{X=\mathrm{VOD},sm_1,sm_2} J(X) = \sum_{t=1}^{N}\sum_{p=H,V}\left(T_b^{obs} - T_b^{model}(X)\right)^2. \quad (2)$$

This approach is generalizable to N overpasses as long as the assumption of constant VOD is met, although only two overpasses are used here to minimize the total time period of each window and to maximize the accuracy of the constant VOD assumption. The robustness of a two-overpass window can be checked using the DoI. A single snapshot of dual-polarized single-incidence angle observations at L-band has a DoI of 1.86 (Konings et al., 2015). This represents the upper limit to how much independent information can be extracted from polarized brightness temperature measurements. Brightness temperatures are also correlated in time, which further reduces the amount of information that can be expected from adjacent (in time) overpasses. With two overpasses the maximal Degree of Information is $2 \times 1.86 = 3.72$. This means that at most three independent may be robustly estimated: one VOD value and two independent soil moisture values. An exception condition is if the brightness temperatures in both polarizations are numerically identical among adjacent overpasses. In such circumstances, there are no longer adequate observation constraints to estimate three variables uniquely and the estimation problem is equivalent to the dual-channel algorithm. Such cases are not filtered from the retrievals presented here. The moving window causes two VOD values to be retrieved for each pixel, time combination: one when that time occurs as the first overpass in the window and once when it is the second (and similarly for soil moisture). The two retrievals are averaged to

produce a single retrieval, with the differences being generally relatively small (Konings et al., 2016).

In addition, the MT-DCA allows for the retrieval of the effective scattering albedo. Changing the effective scattering albedo values in minimizing (2) is changing the forward model $T_b^{model}(X)$. Estimates of effective scattering albedo are obtained by selecting the model (from a vector of M possible ω values) that results in the minimum of the cost function. In this study we assume the albedo is constant across a longer period of time than the VOD, leading to the complete minimization,

$$\min_{\omega} \sum_{j=1}^{M} \min_{X=VOD,sm_1,sm_2} J(X) = \sum_{t=1}^{N} \sum_{p=H,V} \left(T_b^{obs} - T_b^{model}(X)\right)^2 \quad (3)$$

Here, we assume a temporally constant albedo (as in Van de Griend and Owe, 1994; Wigneron et al., 2004) across the full year of data. Robust albedo retrievals over a shorter period may also be feasible as long as the window is long enough to allow robust retrievals. However, the optimal definition of the appropriate window over which albedo is assumed constant depends on the biome and its phenology. For this global study, we assume ω to be characteristic of local vegetation type, so that the window is equal to one year. The analysis of temporal dynamics in albedo is left to follow-up studies with regional focus.

2.2. Application to SMAP

The L-band brightness temperature (horizontal and vertical polarization) used in this study is the enhanced SMAP radiometer products (Chaubell et al., 2016a, 2016b). The period of coverage is one full annual cycle spanning April 1, 2015, to March 31, 2016. The resolution of the SMAP single-look brightness temperatures are about 40 km based on the geometric mean of the major and minor axes defined by the oval containing half of the power (−3 dB) across the SMAP antenna gain. The enhanced SMAP brightness temperature values used in this study are based on the Backus-Gilbert optimal interpolation of the measurements on a 9 km Equal-Area Scalable Earth-2 (EASE2) grid (Chaubell et al., 2016a, 2016b). Due to the overlapping of single-look measurements, the optimal interpolation is capable of a balance reduction of thermal noise and resolution-enhancement relative to the raw −3 dB resolution for each individual footprint. The amount of true resolution enhancements varies across the swath and along-track depending on the amount of overlapping measurements.

The physical temperature of the soil (assumed equal to that of vegetation) is derived in accordance with Baseline SMAP retrievals (SMAP Algorithm Development Team and Science Team, 2016). The effective soil temperature for L-band emission is taken to be a weighted average (following Choudhury et al., 1982 approach) of the NASA Goddard Space Flight Center GEOS-5 forecasts of soil temperatures in the top two model soil layers.

Unlike in the previous application to Aquarius, the MT-DCA is here used to retrieve soil moisture alongside VOD and albedo, rather than the soil dielectric constant. This allows for an explicit study of the effect of the multi-temporal vegetation approach on soil moisture retrievals. The Mironov dielectric mixing model (Mironov et al., 2004) and Fresnel equations are used to relate the soil moisture estimate to the observed smooth surface reflectivity. Clay fraction data used in the dielectric mixing estimates are obtained from several soil datasets, as outlined in (Das and O'Neill, 2010).

The roughness of the soil surface affects the emission from the ground (Wigneron et al., 2017 Table 2 and discussion in Section 3.2). The surface roughness parameters are likely to be dependent on land use and history of precipitation events. Direct measurements of roughness parameters are available only at a few field experiment sites and their mean and temporal changes cannot be mapped globally. For implementation with global L-band retrievals of surface soil moisture, the surface roughness statistics have also been found to be related to land use (Parrens et al., 2016; De Lannoy et al., 2014; Wigneron et al., 2017). In this study we assume a constant roughness root-mean-square height h = 0.13, to avoid the need to use optically-based land use classifications in the retrieval algorithm. The numerical value is close to the median of global values used in O'Neill et al. (2015). Changing the roughness value did not have a significant effect on the retrieved albedo when the MT-DCA was applied to Aquarius data (Konings et al., 2016) as it can trade off with smooth-surface reflectivities, which effect only

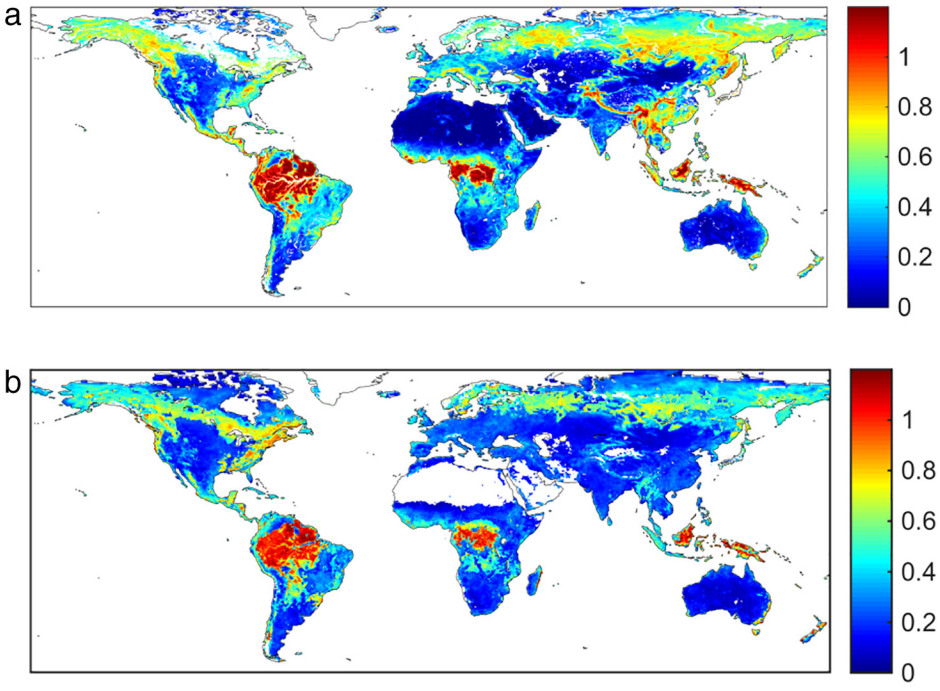

Fig. 1. (a) Global distribution of the time-averaged MT-DCA SMAP vegetation optical depth (dimensionless), calculated across all retrieved values of VOD. (b) Global distribution of the time-averaged SMOS vegetation optical depth τ at nadir (dimensionless), based on angular information.

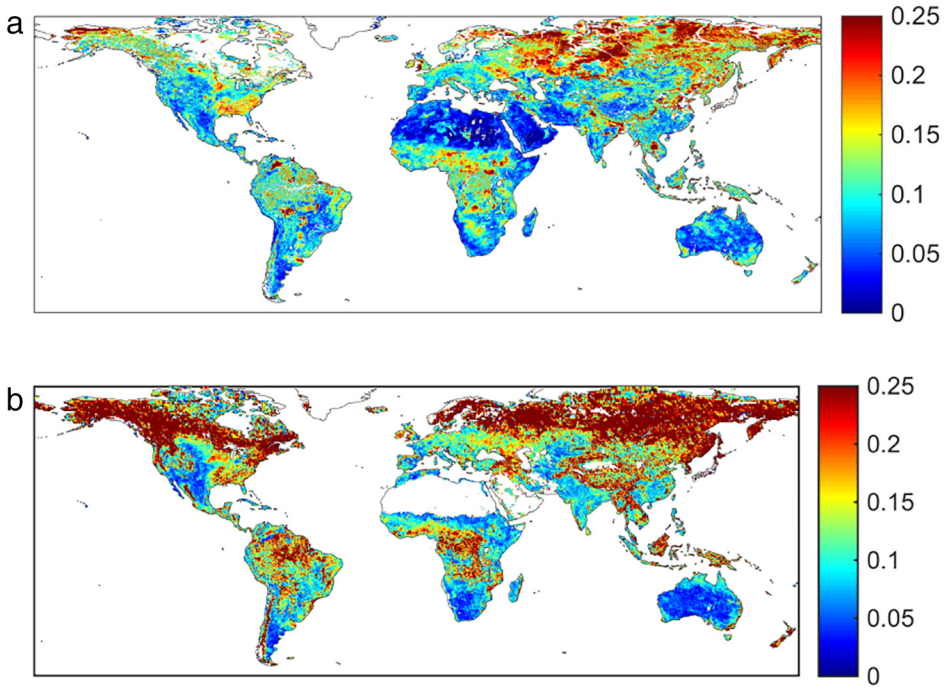

Fig. 2. (a) Global distribution of the seasonal amplitude of vegetation optical depth. A 45-day moving-average filter is applied to define the seasonal cycle. (b) Same as (a) with SMOS retrievals.

the soil moisture and not the vegetation properties of primary interest in this paper. The rough and smooth surface reflectivities are assumed to be related by

$$r_p^{rough} = r_p^{smooth}(sm)\ \exp(-h) \tag{4}$$

Measurements where the physical temperature is <273 K are assumed to cover frozen soils and are not included in this study. Additionally, pixels with >5% water-body presence within an area centered on a 9 km pixel but extending to the −3 dB or 40 km surroundings are also filtered (Chan, 2013a). Lastly, to further enhance the accuracy of the solution, the discretized look-up tables previously used for minimization in (Konings et al., 2016) are now replaced with a simplex search method starting from several random initial conditions.

2.3. Additional datasets used

Several additional data sets are used for interpreting the results. The land cover classification data (according to the International Geosphere-Biosphere Program IGBP categories) are those used by the SMAP project, with full details described in (Kim, 2013). The IGBP classifications are made based on optical Advanced Very High Resolution Radiometer (AVHRR) data. The percentage of each classification is estimated over a 40 km area centered on the 9 km EASE2 grid nodes.

SMOS-derived VOD data from its latest version (L2 v.620) covering the study period are used in this paper. Details about this last re-processing version are given in Kerr et al. (2015). After discarding grid points affected by RFI, a bilinear interpolation is applied to bin the data from its native ISEA 4h9 grid to the scalable EASE2 grid used by SMAP.

The SMAP VOD estimates are also compared to lidar-derived canopy height data from data collected during 2005 by the Geoscience Laser Altimeter System (GLAS) aboard the NASA ICESat (Ice, Cloud, and land Elevation Satellite), with a regression tree algorithm used to fill in values in a few regions with sparse observations (Simard et al., 2011). Similar area-averaging centered on the 9 km EASE2 grid is used to be compatible with the sampling area of the SMAP radiometer.

3. Results

3.1. Vegetation characterization

Fig. 1a shows the time-averaged L-band microwave VOD for the one full annual cycle of SMAP measurements across the globe. The values reach up to 1.2 (top 1 percentile value) over dense tropical forest, which corresponds to a 79% extinction of the emission by the vegetation layer at 40° incidence angle. Globally the median value of VOD is 0.33, which corresponds to 35% extinction. The pattern of average vegetation optical depth in Fig. 1a follows the broad distribution of biomes. Regions of complex topography appear to result in lower VOD. We did not mask out regions of complex topography in this study to learn about its effects on estimation. Tropical forests have the largest values of VOD with a

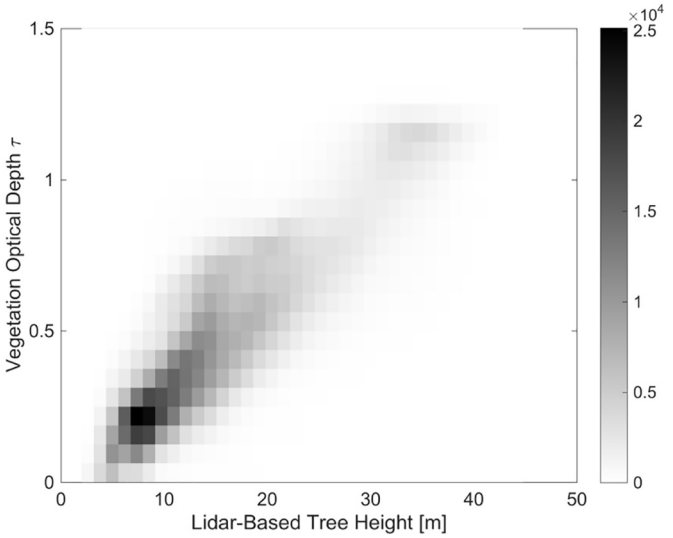

Fig. 3. Joint histogram of time-average vegetation optical depth (from SMAP microwave radiometer measurements) and vegetation height (from GLAS Lidar measurements). The shading is the data count from the global data.

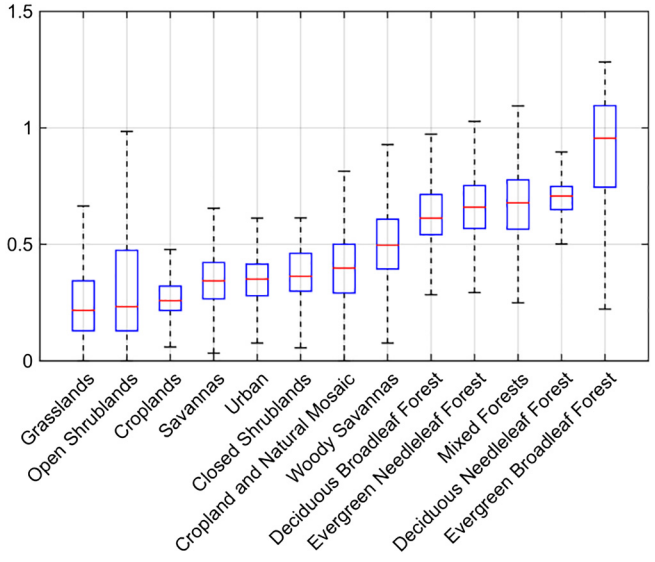

Fig. 4. Box-plots of the time-averaged vegetation optical depth for different IGBP landcover classifications. The data are sorted from left to right in order of increasing median (red line) values. The boxes (blue) mark the extent of the 25th and 75th percentiles. The whiskers extend to the maximum and minimum values. (For interpretation of the references to colour in this figure legend, the reader is referred to the web version of this article.)

distinct difference between dry and wet tropical forests. For example the delineations between dense wet tropical Amazon and the dry tropical forests covering the Nordeste region in Brazil and half of Venezuela are evident. Additionally, the wet tropical forests of central Africa are sharply delineated from the Zambian and other dry tropical forests in Angola. Across northern India, Nepal and parts of northern Pakistan, estimates of VOD are large. Sloping terrain may contribute to errors in retrievals over this region. In North America the deciduous forests along the Eastern United States are characterized by intermediate values of VOD whereas the Great Plains and Prairies extending into Canada have distinct lower values. In boreal regions, the dense Taiga forests across Russia and Central Asia values up to 0.80 represent up to 65% canopy extinction of surface emission. Further north in the Tundra region, VOD is reduced again, likely due to the low fractional coverage of the canopy there. For comparison, Fig. 1b shows VOD estimates from SMOS v.620. This estimate is based on the angular information in the brightness temperatures observed by the SMOS radiometer. In its latest version, the forest modeling has undergone significant improvements and provides more realistic values of forest opacity, which now enables in many cases retrieval of soil moisture below forest canopies (Vittucci et al., 2016). Even though the two instruments use different information on the polarized L-band emission from the surface and have different retrieval approaches, they yield comparable patterns of opacity across the globe. The SMAP estimates tend to reach higher values in dense tropical forests (up to 1.2), in boreal North America and Asia. This may be due to the use of prior values from optical measurements in the SMOS algorithm for retrieval initial guess and also due to a reduction in polarization and incidence angle information over dense vegetation. Also, the SMOS L2 processor only retrieves the VOD of the dominant cover (low vegetation or forest, according to a high resolution land cover map) (Kerr et al., 2012), and this can lead to differences between the two VOD retrievals, particularly in mixed pixels. Perhaps the biggest difference between SMOS and SMAP VOD estimates occurs in Southeast Asia, where SMOS values are relatively low (<0.4) but SMAP values are generally >0.6, with the main differences occurring in Southeastern China. This can be due to the fact that, in this particular region, the RFI observed by the SMOS satellite exceeds expected levels (Oliva et al., 2016). In general, the global patterns of SMAP VOD differ from those of solar-induced fluorescence (Guanter et al., 2014) or land cover (Arino et al., 2000).

To further analyze the VOD dynamics, Fig. 2a shows the seasonal amplitude of VOD, which depends on plant phenology. The seasonal cycle is estimated by applying a 45-day sliding-average window to the data. A 45-day window maintained the amplitude of the annual cycle in most locations while removing individual spikes in the VOD time-series. In calculating this moving window average, the data are treated as periodic in order to allow estimation at the beginning and end of the record. The seasonal amplitude is the difference between the peak and trough of VOD time-series after the sliding-average window application. The VOD amplitude appears to be highest for regions with light-limitation in vegetation phenology. These include deciduous forests (such as those in the southeastern United States) and broad boreal regions. The dry tropical savannah regions in Africa and South America also have large seasonal cycle amplitude, though their seasonality is driven by water rather than light limitation. Fig. 2b shows the seasonal amplitude based on the SMOS VOD retrievals. In the boreal and tropical dense forested regions, the amplitude is higher than the one derived from SMAP. In the transition zones and less vegetated regions, the amplitudes are comparable.

Additional support for the global distribution of VOD is provided by a comparison to vegetation height estimates from the GLAS. Fig. 3 shows the joint distribution of both. Across the range of both VOD and vegetation height there is strong correspondence between the two (R^2 statistic equal to 0.83 for all global land pixels). This is expected – taller canopies generally have higher biomass values and thus a higher water content. Vittucci et al. (2016) also compared SMOS VOD retrievals and the GLAS lidar tree height over several regions around the globe where the forest vegetation classification was the dominant category or above 50% of the area (see their Figs. 4 and 7 for South America, Fig. 5 for Africa, Fig. 6 for Asia and Figs. 8 and 9 for North America). The GLAS lidar tree height data mostly explained between 60% and 70% of the variance in the distribution of SMOS VOD retrievals mean maps

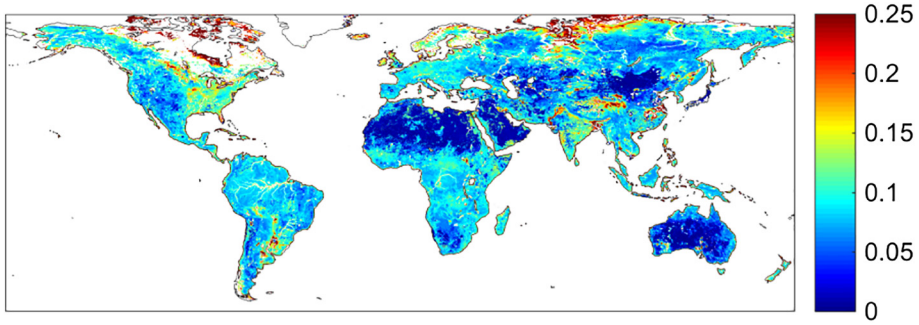

Fig. 5. Retrievals of the effective scattering albedo ω (dimensionless) based on one year of SMAP radiometer measurements and the multi-temporal dual-channel algorithm.

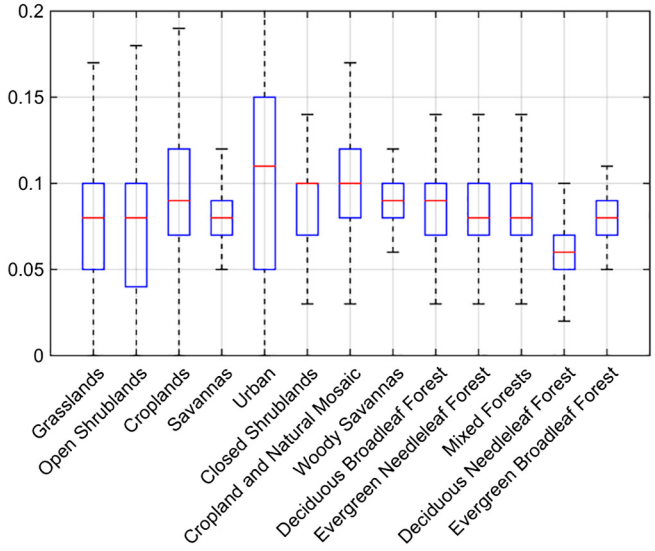

Fig. 6. Boxplots of the effective scattering albedo segmented by the IGBP landcover classification. Neither optical measurement-based IGBP classifications nor the attenuation of the microwave radiation uniquely and distinguishably associate with a range of effective scattering albedo.

(Tables 2 and 3 in Vittucci et al. (2016)), slightly less than for the SMAP MT-DCA VOD.

Fig. 4 shows boxplots of the distribution of VOD within each biome classification. Biomes are sorted by increasing median values of VOD. Grasslands and croplands as well as open shrublands have the lowest values of VOD relative to regions with woody vegetation. Forests and more woody vegetation biomes consistently have the higher values of microwave vegetation optical depth, in line with previous findings from a validation study of AMSR-E VOD using in situ biomass in the Sahel (Tian et al., 2016b). The evergreen broadleaf forests (wet tropics) consistently have the highest values of VOD as expected. Interestingly, the distribution of VOD is among the most narrow for croplands, despite the wide variety of planting densities employed across regions, and differences in biomass and hydraulic behavior between different crop types.

The effective scattering albedo map based on the one full annual cycle of SMAP measurements is shown in Fig. 5. The effective scattering albedo is characterized by a median of 0.08 and the interquantile range is 0.05. The estimated median values of the effective scattering albedo are all above 0.05 and are higher than those used in SMAP (see Table III of Chan et al. (2016)) and SMOS Baseline retrieval algorithms (0.0 globally except 0.08 for boreal forests and 0.06 for other forest types. See Wigneron et al., 2017 Table 2). It is noteworthy that the recent SMOS-IC product also reports considerably higher effective scattering albedo values after calibration with in situ soil moisture observations (see Table 1 in Fernandez-Moran et al. (2017)).

Two-thirds of the retrieved ω values are below 0.1. Only 5% of the pixels attain values >0.17 and these are mostly in the far northern regions of Canada and the Tundra. However, over these regions, inland water bodies and seasonally frozen ground may affect estimation and should be treated with caution. Although we have attempted to account for both (see methods), the detection of frozen soils and small (possibly seasonal) water bodies is likely imperfect. Interestingly the map of ω shows concentrated regions of high values (outside of boreal regions) in regions of intensive and wide-spread agriculture, such as in the upper Midwest US, northern Argentina, Indus Valley and other smaller regions. This is reflected in the boxplots of ω by land cover type shown in Fig. 6 - agricultural regions, shrublands and savannahs have the highest values of albedo (urban regions cannot be interpreted). Heterogeneity of vegetation appears to contribute to high effective albedo retrievals. In essence, vegetation heterogeneity may be acting like complex structural geometry when viewed effectively over the large field-of-view. Fig. 7 shows that the mean value of the effective scattering albedo consistently increases with the degree of landscape heterogeneity. The Gini-Simpson Index (GSI) commonly used in ecology – is a measure of degree of heterogeneity. It is computed as the complement of the sum of squared N-member fractions of landscape composition:

$$GSI = 1 - \sum_{i=1}^{N} f_i^2$$

where f_i is the fraction of the area covered by the i-th land use classification. In this calculation we use the −3 dB half-power area (about 40 km) centered on the 9 km grid as the total area represented by the SMAP brightness temperature estimates. Although there is considerable scatter within each GSI class, the effective scattering does increase with degree of heterogeneity in the landscape. As expected based on the spatial distributions in Figs 1a and 5, the joint distribution of temporally averaged VOD and ω do not show a consistent relationship (Fig. 8). The joint distribution was also estimated within IGBP classes (not shown) and no distinct patterns were evident. This is consistent with the

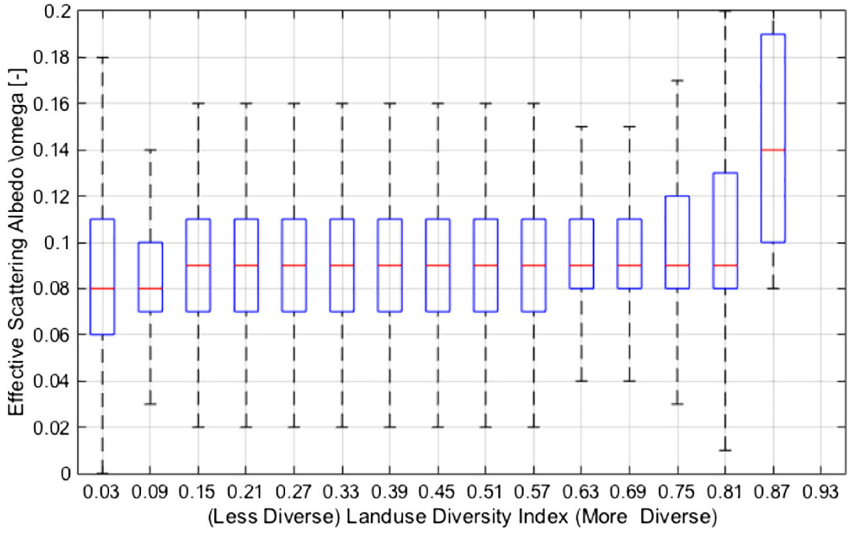

Fig. 7. The boxplot distribution of effective scattering albedo for different degrees of land use heterogeneity as represented by the Gini-Simpson Diversity Index. More heterogeneity results in upward shifts of the effective scattering albedo median and distributions.

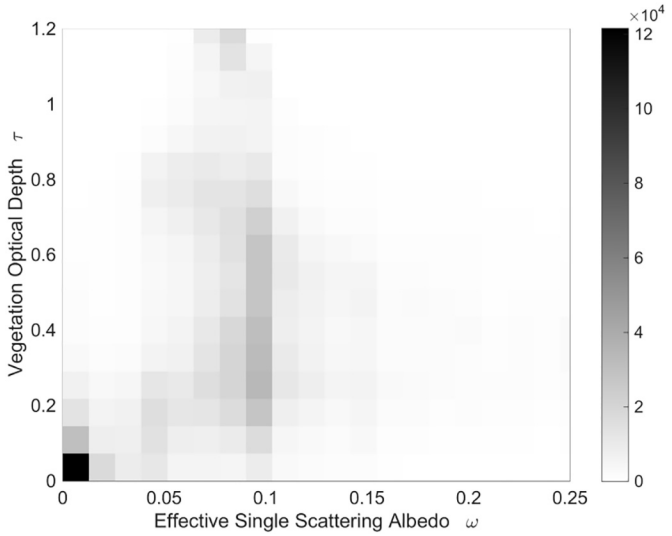

Fig. 8. Joint histogram of time-average retrieved vegetation optical depth and effective scattering albedo based on one year of SMAP radiometer measurements and application of the multi-temporal dual-channel algorithm. There is no discernable and consistent relationship between the attenuation and scattering properties of vegetation.

different physical properties reflected in these retrievals. The VOD is related to the extinction due to the canopy layer and thus to the integrated wet biomass of the canopy, while the ω is related to the structure of the canopies and the landscape.

3.2. Impacts on soil moisture estimation

The vegetation parameters also have an impact on the estimation of surface soil volumetric water content. Here, we assess the impact of the MT-DCA approach on retrieved soil moisture by comparing MT-DCA retrievals to those of the Baseline algorithm used by the SMAP team. The Baseline radiometer-only algorithm uses a semi-empirical formula for VWC based on land cover type and the seasonal climatology of the optical NDVI (O'Neill et al., 2015). The VWC is then converted to VOD by a constant parameter b that is also based on land cover classification (O'Neill et al., 2015). The albedo ω is once again dependent on land cover. Neither the Baseline algorithm nor the implementation of the tau-omega model here consider the possible polarization dependence of the vegetation parameters, in favor of parsimony. Using these ancillary vegetation parameter estimates, the Baseline algorithm is a single-channel algorithm that minimizes the cost function mismatch of the V-polarized brightness temperatures of a single time snapshot. The two implementations of the r_p^{Rough} inversion for volumetric soil water content are identical in terms of roughness and soil dielectric constant models.

Fig. 9 shows the global map of mean retrieved surface volumetric soil water content from the MT-DCA for the study period. The broad distribution of surface volumetric soil moisture content is similar to that of the Baseline algorithm for the same one-year period of record. Figs. 10 to 12 show the difference between the two soil moisture retrievals, decomposed into the unbiased root-mean-square difference (which is sensitive to the amplitude of random errors), temporal correlation (sensitive to temporal consistency), and mean offset or biases (Entekhabi et al., 2010).

Fig. 10 is the map of ubRMSE between the retrieved soil moisture in this study and the Baseline SMAP radiometer-only product (O'Neill et al., 2015). The random differences are remarkably low - less than 0.01 cm^3/cm^3 over most of the globe (i.e., the third digit on the units for the variable). This suggests that the temporal variability of the retrievals is primarily driven by variations in the SMAP brightness temperature, which is of course identical for both cases. Notable exceptions with large ubRMSE between the retrievals can be found in several tropical agricultural regions (e.g., northern Argentina, parts of South Asia) and vegetation transition zones such as Sahelo-Soudan in West Africa. Even in these regions of high ubRMSE, the difference is small relative to the SMAP retrieval error target of 0.04 cm^3/cm^3.

The correlation coefficient between the two estimates of soil water content over most of the global land surfaces is above 0.95, with the exception of wet tropical forests and boreal regions (Fig. 11). Over the latter two biomes, the high VOD in these regions corresponds to large vegetation attenuation and low sensitivity to soil moisture, such that even small retrieval differences translate to large amplitude errors in volumetric soil water content. Indeed, the Amazon wet tropical forest, central Africa tropical forest and southeast Asia forests are evident on the map as regions with relatively lower correlation closer to $R = 0.75$. However over less dense vegetated surface and much of the remainder of global land area, the correlation is high indicating good correspondence of temporal variations.

Larger and more noticeable differences appear in the mean bias statistics. The bias is estimated over the full annual cycle and is defined as the soil moisture estimates from O'Neill et al. (2016) minus the estimates from the MT-DCA algorithm of this study. Fig. 12a shows the mean bias between the two data sets. The bias differences are many times greater than the ubRMSD difference, especially over wet tropical forests and the eastern half of North America where the MT-DCA soil moisture is biased by up to 0.1 $cm^3\ cm^{-3}$ relative to the Baseline algorithm. The opposite-sign bias is evident over the boreal regions where the Baseline retrievals are drier by about 0.1 $cm^3\ cm^{-3}$. The cause of the pattern is evident in the bias in VOD (Fig. 12b). The average VOD estimated from the semi-empirical relationship to optical data (from O'Neill et al., 2016) is larger over the wet tropical forests (by up to 0.2) and lower by >0.2 over boreal regions. When VOD is over-

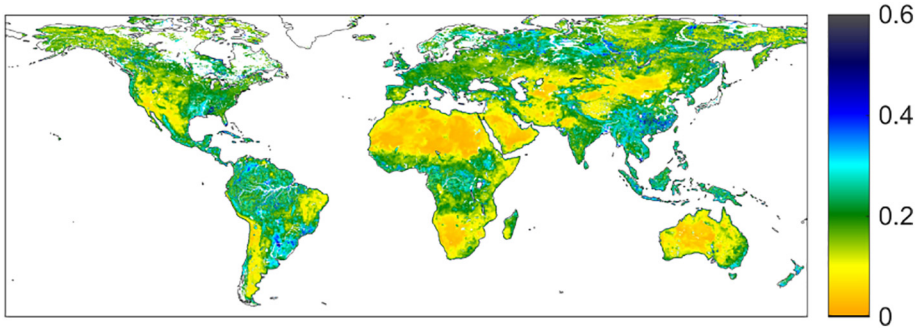

Fig. 9. The global distribution of time-average retrieved surface soil moisture based on one year of SMAP radiometer observations and application of the multi-temporal dual-channel algorithm.

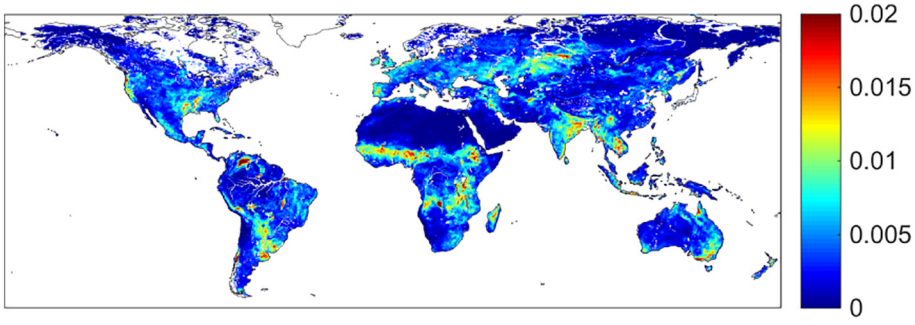

Fig. 10. Statistical comparison of the single-channel V-pol SMAP Baseline surface soil moisture retrievals (O'Neill et al., 2016) and the multi-temporal dual channel retrievals. The unbiased (bias-removed) root mean-squared (ubRMSE) difference captures the amplitude of the time-varying random errors between two data sets.

estimated, the emission from the vegetation is over-estimated but the attenuation of soil surface emission is also larger. Depending on the soil and vegetation parameter values, this can lead to lower estimates for the same brightness temperatures as apparent in the biases reported in Fig. 11. Colder brightness temperature estimates for the soil contribution drive retrievals of surface volumetric soil water content higher. The opposite sequence applies to when VOD is under-estimated. It should be noted that because only a single year of SMAP data are available, these datasets cannot be used to study the additional impact of the missing interannual variability in the prior estimates used for VOD in the SMAP Baseline algorithm.

The SMAP Baseline product has been validated extensively against in situ measurements at both a limited number of core validation sites and several hundred sparse network points (Chan et al., 2016). The same has been applied to O'Neill et al. (2016) 9 km product with very similar results. These sites are mostly located in the United States and Canada with very limited numbers in Australia, Europe and limited sites in Asia, Africa and South America, over which the ubRMSD between the sites is $<0.01\ cm^3\ cm^{-3}$. Unfortunately, there are no reliable networks of in situ measurements to investigate the tropical and boreal regions where differences between the soil moisture retrievals from MT-DCA and the Baseline algorithms are larger. In the future, global evaluation of the errors associated with using empirical VOD and albedo estimates in soil moisture retrieval could be achieved using triple collocation (McColl et al., 2014a; Gruber et al., 2015). However, a longer record of SMAP measurements than is presently available is necessary to apply this technique (Yilmaz and Crow, 2014). Furthermore, though triple collocation may be useful for evaluating the differences in soil moisture ubRMSD between the MT-DCA and the Baseline SMAP algorithm, it is not able to determine bias levels.

4. Conclusions

In this study, we apply the multi-temporal dual-channel algorithm to retrieve microwave vegetation optical depth and surface soil moisture as well as to estimate the effective scattering albedo from the first full year of SMAP L-band radiometric observations. The vegetation optical depth is assumed to be slowly varying and the same in two time-adjacent overpasses (two to three days apart). Surface soil moisture can be different for every overpass. The effective scattering albedo is also estimated but assumed fixed for the period of record. The temporal average of the global vegetation microwave optical depth follows biome patterns and has a strong positive correspondence to lidar-based estimates of canopy height. The global median VOD is about 0.33 which corresponds to a 35% extinction at the 40° incidence angle value of SMAP. The global mean values of L-band multi-temporal SMAP-based VOD are also comparable to current SMOS VOD retrievals based on multi-angular information. However, the SMAP mean VOD fields have a slightly higher dynamic range when compared to SMOS-derived values and the seasonal amplitude of the two retrievals is noticeably different in boreal and tropical forests. The loss of polarization difference with increasing vegetation density and the role of incidence angle in modulating this effect may be a contributing factor to this difference. Another factor may be the reduction of brightness temperature range over dense vegetation, or significant changes in VOD over the moving window due to changes in vegetation water stress in tropical forests during the 2015/2016 El Nino event (Jiménez-Muñoz et al., 2016), which will affect the effectiveness of separation of time-scales used in this study. Further research is needed, though care should be taken in interpreting these differences as the SMOS team is also working on a new VOD product. In the forthcoming SMOS-IC algorithm, optical data are no longer used in estimating VOD (Fernandez-Moran et al., 2017).

The albedo values have a median value of 0.08 but have a long tail with very high values in boreal regions which is higher than the values commonly used for both the SMAP and SMOS Baseline products. Interestingly, results indicate that landscapes with high sub-pixel vegetation heterogeneity lead to higher effective scattering albedo retrievals.

Explicit validation of VOD by comparison to in situ is significantly more challenging than validation of soil moisture. Confidence in the

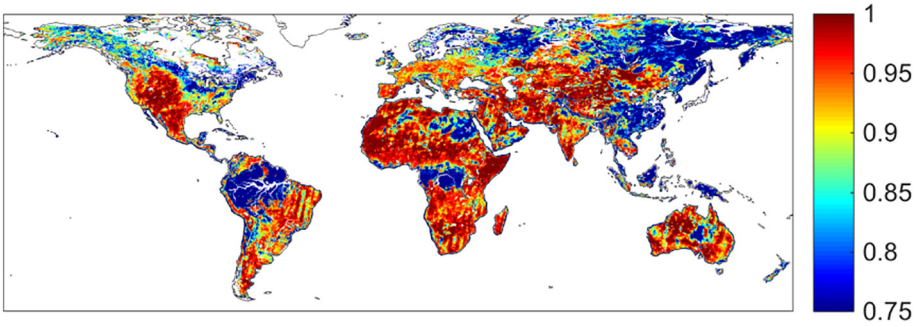

Fig. 11. The correlation map values are mostly above 0.95 except for dense tropical forests where it can be as low as 0.75. The correlation captures phase correspondence between two data sets regardless of amplitude and off-set differences.

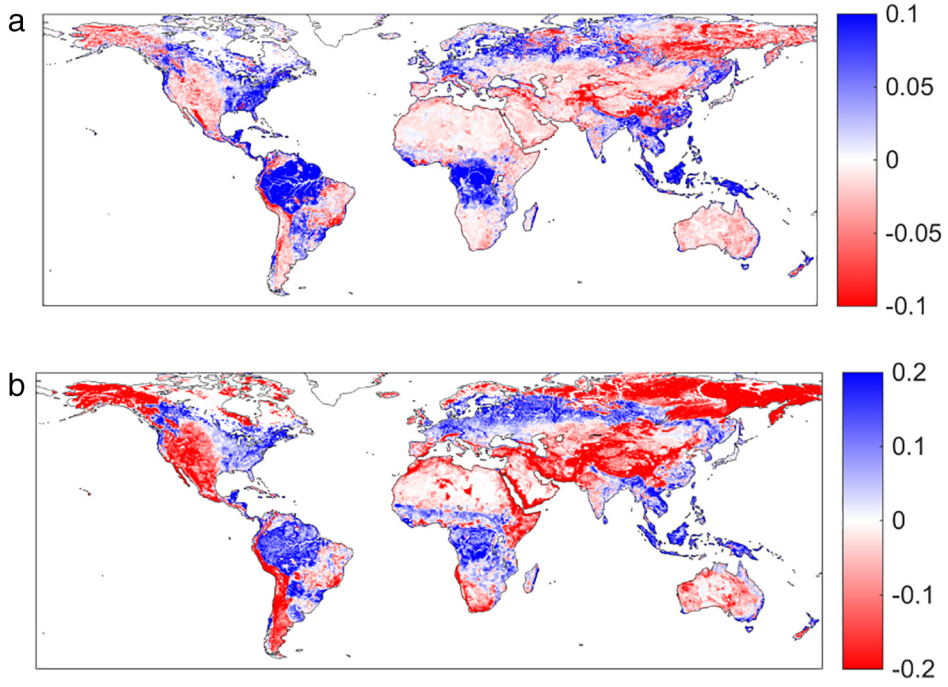

Fig. 12. (a) Bias in soil moisture between the SMAP Baseline retrieval algorithm and the retrievals based on the algorithm in this study (single-channel V-pol in O'Neill et al. (2016) minus the multitemporal dual-channel) over one full seasonal cycle of record. (b) Same as (a) for vegetation opacity VOD.

VOD retrievals can be obtained from indirect evidence regarding the expected patterns of seasonal cycles with collocated precipitation as well as soil moisture series (Konings et al., 2016). Nevertheless, with the exception of (Tian et al., 2016b), VOD products have seen little validation, and to the authors' knowledge, no VOD algorithm comparison has been able to compare to ground based data.

Soil moisture retrievals were also investigated by comparing them to soil moisture retrievals from the Baseline SMAP algorithm, a V-polarized single-channel algorithm that uses prior albedo and VOD estimates based on land cover and NDVI. The unbiased RMSD difference between MT-DCA and Baseline soil moisture retrievals was generally small (<0.01) over most of the world, with exceptions in agricultural regions in India and Argentina, California, and in the Sahel and dry tropical forests in Africa. Correlation coefficient were high ($R > 0.75$) globally but lowest in the tropical forests, likely reflecting the different approaches to account for attenuation of L-band soil emissivity through the very dense vegetation. However, soil moisture mean biases were high in many global regions, including not just the regions of low correlations but also forests in the Eastern US, grasslands and croplands in Central Asia, Southeastern China, and Central Europe. The spatial patterns of the soil moisture biases reflect biases between the MT-DCA and SMAP Baseline VOD estimates, suggesting a dominant role of VOD over albedo in its effect on the soil moisture retrieval bias.

Acknowledgments

Code and data are available from the authors upon request.

References

Andela, N., Liu, Y.Y., van Dijk, A.I.J.M., de Jeu, R.A.M., McVicar, T.R., 2013. Global changes in dryland vegetation dynamics (1988–2008) assessed by satellite remote sensing: comparing a new passive microwave vegetation density record with reflective greenness data. Biogeosciences 10 (10):6657–6676. http://dx.doi.org/10.5194/bg-10-6657-2013.

Arino, O., Arino, O., Gross, D., Gross, D., Ranera, F., Ranera, F., 2000. GlobCover: ESA service for global land cover from MERIS. Processing, pp. 2412–2415.

Barichivich, J., Briffa, K.R., Myneni, R.B., Osborn, T.J., Melvin, T.M., Ciais, P., Piao, S., Tucker, C., 2013. Large-scale variations in the vegetation growing season and annual cycle of atmospheric CO_2 at high northern latitudes from 1950 to 2011. Glob. Chang. Biol. 19 (10):3167–3183. http://dx.doi.org/10.1111/gcb.12283.

Chan, S., 2013a. SMAP Ancillary Data Report: Static Water Fraction. Jet Propulsion Laboratory, California Institute of Technology, Pasadena, CA, p. JPLD-53059.

Chan, S., 2013b. SMAP Ancillary Data Report: Vegetation Water Content. Jet Propuls. Lab. Calif. Inst. Technol., JPL, p. D047.

Chan, S.K., et al., 2016. Assessment of the SMAP passive soil moisture product. IEEE Trans. Geosci. Remote Sens. 54 (8):4994–5007. http://dx.doi.org/10.1109/TGRS.2016.2561938.

Chaubell, J., Yueh, S., Entekhabi, D., Peng, J., 2016a. Resolution enhancement of SMAP radiometer data using the Backus Gilbert optimum interpolation technique. 2016 IEEE Int. Geosci. Remote Sens. Symp:pp. 284–287. http://dx.doi.org/10.1109/IGARSS.2016.7729065.

Chaubell, M.J., Chan, S., Dunbar, R.S., Peng, J., Yueh, S., 2016b. SMAP Enhanced L1C Radiometer Half-Orbit 9 km EASE-Grid Brightness Temperatures, Version 1. http://dx.doi.org/10.5067/2C9O9KT6JAWS.

Choudhury, B., Schmugge, T., Mo, T., 1982. A parameterization of effective soil temperature for microwave emission. J. Geophys. Res. 87, 1301–1304.

Crow, W.T., Chan, S.T.K., Entekhabi, D., Houser, P.R., Hsu, A.Y., Jackson, T.J., Njoku, E.G., O'Neill, P.E., Shi, J., Zhan, X., 2005. An observing system simulation experiment for Hydros radiometer-only soil moisture products. IEEE Trans. Geosci. Remote Sens. 43 (6):1289–1303. http://dx.doi.org/10.1109/TGRS.2005.845645.

Das, N., O'Neill, P., 2010. Selection of Soil Attributes Datasets for the SMAP Mission, SMAP Science Document #D-53058, 1.1, JPL, Dec., 2010.

De Lannoy, G.J.M., Reichle, R.H., Vrugt, J.A., 2014. Uncertainty quantification of GEOS-5 L-band radiative transfer model parameters using Bayesian inference and SMOS observations. Remote Sens. Environ. 148, 146–157.

Du, J., Kimball, J.S., Jones, L.A., Member, S., 2015. Passive microwave remote sensing of soil moisture based on dynamic vegetation scattering properties for AMSR-E. IEEE Trans. Geosci. Remote Sens. 1–12.

Entekhabi, D., Reichle, R.H., Koster, R.D., Crow, W.T., 2010. Performance metrics for soil moisture retrievals and application requirements. J. Hydrometeorol. 11 (3): 832–840. http://dx.doi.org/10.1175/2010JHM1223.1.

Entekhabi, D., Yueh, S., O'Neill, P., Kellogg, K.H., Al, E., 2014. SMAP Handbook.

Fernandez-Moran, R., Al-Yaari, A., Mialon, A., Mahmoodi, A., Al Bitar, A., De Lannoy, G., Rodriguez-Fernandez, N., Lopez-Baeza, E., Kerr, Y., Wigneron, J.-P., 2017. SMOS-IC: an alternative SMOS soil moisture and vegetation optical depth product. Remote Sens. 9:457. http://dx.doi.org/10.3390/rs9050457.

Grant, J.P., Wigneron, J.-P., De Jeu, R.A.M., Lawrence, H., Mialon, A., Richaume, P., Al Bitar, A., Drusch, M., Van Marle, M.J.E., Kerr, Y., 2016. Comparison of SMOS and AMSR-E vegetation optical depth to four MODIS-based vegetation indices. Remote Sens. Environ. 172, 87–100.

Gruber, A., Su, C.-H., Zwieback, S., Crow, W., Dorigo, W., Wagner, W., 2015. Recent advances in (soil moisture) triple collocation analysis. Int. J. Appl. Earth Obs. Geoinf. http://dx.doi.org/10.1016/j.jag.2015.09.002.

Guan, K., Wolf, A., Medvigy, D., Caylor, K.K., Pan, M., Wood, E.F., 2013. Seasonal coupling of canopy structure and function in {A}frican tropical forests and its environmental controls. Ecosphere 4 (3) (art35–, doi:10.1890/ES12-00232.1).

Guan, K., Wood, E.F., Medvigy, D., Kimball, J., Pan, M., Caylor, K.K., Sheffield, J., Xu, X., Jones, M.O., 2014. Terrestrial hydrological controls on land surface phenology of African savannas and woodlands. J. Geophys. Res. Biogeosci. 119:1652–1669. http://dx.doi.org/10.1002/2013JG002572.

Guanter, L., et al., 2014. Global and time-resolved monitoring of crop photosynthesis with chlorophyll fluorescence. Proc. Natl. Acad. Sci. 111 (14):E1327–E1333. http://dx.doi.org/10.1073/pnas.1320008111.

Hellkvist, J., R., G.P., J., P.G., 1974. Vertical gradients of water potential and tissue water relations in sitka spruce trees measured with the pressure chamber. J. Appl. Ecol. 11 (2), 637.

Jackson, T., Schmugge, T., 1991. Vegetation effects on the microwave emission of soils. Remote Sens. Environ. 36 (3), 203–212.

Jiménez-Muñoz, J.C., Mattar, C., Barichivich, J., Santamaría-Artigas, A., Takahashi, K., Malhi, Y., Sobrino, J.A., van der Schrier, G., 2016. Record-breaking warming and extreme drought in the Amazon rainforest during the course of El Niño 2015–2016. Sci Rep 6 (May):33130. http://dx.doi.org/10.1038/srep33130.

Jones, L.A., Ferguson, C.R., Kimball, J.S., Zhang, K., Chan, S.T.K., McDonald, K.C., Njoku, E.G., Wood, E.F., 2010. Satellite microwave remote sensing of daily land surface air temperature minima and maxima from AMSR-E. IEEE J. Sel. Top. Appl. Earth Obs. Remote Sens. 3 (1):111–123. http://dx.doi.org/10.1109/JSTARS.2010.2041530.

Jones, M.O., Jones, L.A., Kimball, J.S., McDonald, K.C., 2011. Satellite passive microwave remote sensing for monitoring global land surface phenology. Remote Sens. Environ. 115 (4):1102–1114. http://dx.doi.org/10.1016/j.rse.2010.12.015.

Jones, M.O., Kimball, J.S., Jones, L.A., McDonald, K.C., 2012. Satellite passive microwave detection of North America start of season. Remote Sens. Environ. 123 (0):324–333. http://dx.doi.org/10.1016/j.rse.2012.03.025.

Kerr, Y.H., Njoku, E.G., 1990. A semiempirical model for interpreting microwave emission from semiarid land surfaces as seen from space. IEEE Geosci. Remote Sens. Lett. 28 (3), 384–393.

Kerr, Y.H., et al., 2010. The SMOS mission: new tool for monitoring key elements of the global water cycle. Proc. IEEE 98 (5):666–687. http://dx.doi.org/10.1109/JPROC.2010.2043032.

Kerr, Y.H., Waldteufel, P., Richaume, P., Wigneron, J.-P., Ferrazzoli, P., Mahmoodi, A., Al Bitar, A., Cabot, F., Gruhier, C., Juglea, S.E., Leroux, D., Mialon, A., Delwart, S., 2012. The SMOS soil moisture retrieval algorithm. IEEE Trans. Geosci. Remote Sens. 50, 1384–1403.

Kerr, Y.H., Waldteufel, P., Richaume, P., Ferrazzoli, P., Wigneron, J.-P., 2015. SMOS level 2 processor soil moisture algorithm theoretical basis document (ATBD): SO-TN-ARR-L2PP-0037 v3.9. Toulouse, SM-ESL (CBSA). https://earth.esa.int/web/guest/-/data-processors-7632.

Kim, S., 2013. SMAP Ancillary Data Report on Landcover Classification. Jet Propuls. Lab. Calif. Inst. Technol., JPL, p. D-53057.

Konings, A.G., Gentine, P., 2017. Global variations in ecosystem-scale isohydricity. Glob. Chang. Biol. 23:891–905. http://dx.doi.org/10.1111/gcb.13389.

Konings, A.G., Entekhabi, D., Chan, S.K., Njoku, E.G., 2011. Effect of radiative transfer uncertainty on L-band radiometric soil moisture retrieval. IEEE Trans. Geosci. Remote Sens. 49 (7):2686–2698. http://dx.doi.org/10.1109/TGRS.2011.2105495.

Konings, A.G., McColl, K.A., Piles, M., Entekhabi, D., 2015. How many parameters can be maximally estimated from a set of measurements? IEEE Geosci. Remote Sens. Lett. 12 (5). http://dx.doi.org/10.1109/LGRS.2014.2381641.

Konings, A.G., Piles, M., Rotzer, K., McColl, K.A., Chan, S.K., Entekhabi, D., 2016. Vegetation optical depth and scattering albedo retrieval using time series of dual-polarized L-band radiometer observations. Remote Sens. Environ. 172:178–189. http://dx.doi.org/10.1016/j.rse.2015.11.009.

Konings, A.G., Williams, A.P., Gentine, P., 2017. Sensitivity of grassland productivity to aridity controlled by stomatal and xylem regulation. Nat. Geosci. 10:284–288. http://dx.doi.org/10.1038/ngeo2903.

Kurum, M., 2013. Quantifying scattering albedo in microwave emission of vegetated terrain. Remote Sens. Environ. 129 (0), 66–74.

Kurum, M., O'Neill, P.E., Lang, R.H., Joseph, A.T., Cosh, M.H., Jackson, T.J., 2012. Effective tree scattering and opacity at L-band. Remote Sens. Environ. 118 (0), 1–9.

Lawrence, H., Wigneron, J.-P., Richaume, P., Novello, N., Grant, J., Mialon, A., Al Bitara, A., Merlin, O., Guyon, D., Leroux, D., 2014. Comparison between SMOS vegetation optical depth products and MODIS vegetation indices over crop zones of the USA. Remote Sens. Environ. 140 (0):396–406. http://dx.doi.org/10.1016/j.rse.2013.07.021.

Le Vine, D.M., Lagerloef, G.S., Torrusio, S., 2010. Aquarius and remote sensing of sea surface salinity from space. Proc. IEEE 98 (5), 688–703.

Liu, Y.Y., de Jeu, R.A.M., McCabe, M.F., Evans, J.P., van Dijk, A.I.J.M., 2011. Global long-term passive microwave satellite-based retrievals of vegetation optical depth. Geophys. Res. Lett. 38 (18), L18402.

Liu, Y.Y., Evans, J.P., McCabe, M.F., de Jeu, R.A.M., van Dijk, A.I.J.M., Dolman, A.J., Saizen, I., 2013. Changing climate and overgrazing are decimating Mongolian steppes. PLoS One 8 (2):4–9. http://dx.doi.org/10.1371/journal.pone.0057599.

Liu, Y.Y., van Dijk, A.I.J.M., de Jeu, R.A.M., Canadell, J.G., McCabe, M.F., Evans, J.P., Wang, G., 2015. Recent reversal in loss of global terrestrial biomass. Nat. Clim. Chang. 5 (May): 470–474. http://dx.doi.org/10.1038/nclimate2581.

Matzler, C., 1994. Microwave transmissivity of a forest canopy: experiments made with a beech. Remote Sens. Environ. 48 (2):172–180. http://dx.doi.org/10.1016/0034-4257(94)90139-2.

McColl, K.A., Vogelzang, J., Konings, A.G., Entekhabi, D., Piles, M., Stoffelen, A., 2014a. Extended triple collocation: estimating errors and correlation coefficients with respect to an unknown target. Geophys. Res. Lett. 41 (17). http://dx.doi.org/10.1002/2014GL061322.

McColl, K.A., Entekhabi, D., Piles, M., 2014b. Uncertainty analysis of soil moisture and vegetation indices using aquarius scatterometer observations. IEEE Trans. Geosci. Remote Sens. 52 (7), 4259–4272.

Meesters, A.G.C.A., de Jeu, R.A.M., Owe, M., 2005. Analytical derivation of the vegetation optical depth from the microwave polarization difference index. IEEE Geosci. Remote Sens. Lett. 2 (2), 121–123.

Mironov, V.L., Dobson, M.C., Kaupp, V.H., Komarov, S.a., Kleshchenko, V.N., 2004. Generalized refractive mixing dielectric model for moist soils. IEEE Trans. Geosci. Remote Sens. 42 (4):773–785. http://dx.doi.org/10.1109/TGRS.2003.823288.

Mohammed, P.N., Aksoy, M., Piepmeier, J.R., Johnson, J.T., Bringer, A., 2016. SMAP L-band microwave radiometer: RFI mitigation prelaunch analysis and first year on-orbit observations. IEEE Trans. Geosci. Remote Sens. 54 (10):6035–6047. http://dx.doi.org/10.1109/TGRS.2016.2580459.

Njoku, E.G., Ashcroft, P., Chan, T.K., Li, L., 2005. Global survey and statistics of radio-frequency interference in AMSR-E land observations. IEEE Trans. Geosci. Remote Sens. 43 (5):938–946. http://dx.doi.org/10.1109/TGRS.2004.837507.

Oliva, R., Daganzo, E., Richaume, P., Kerr, Y.H., Cabot, F., Soldo, Y., Anterrieu, E., Reul, N., Gutierrez, A., Barbosa, J., Lopes, G., 2016. Status of radio frequency interference (RFI) in the 1400–1427 MHz passive band based on six years of SMOS mission. Remote Sens. Environ. 180, 64–75.

O'Neill, P.E., Njoku, E.G., Jackson, T.J., Chan, S., Bindlish, R., 2015. SMAP Algorithm Theoretical Basis Document: Level 2 & 3 Soil Moisture (Passive) Data Products. Jet Propuls. Lab. Calif. Inst. Technol., JPL, p. D-66480.

O'Neill, P.E., Chan, S., Njoku, E.G., Jackson, T., Bindlish, R., 2016. SMAP Enhanced L3 Radiometer Global Daily 9 km EASE-Grid Soil Moisture, Version 1. NASA National Snow and Ice Data Center Distributed Active Archive Center, Boulder, Colorado USA http://dx.doi.org/10.5067/ZRO7EXJ8O3XI (February 2017).

Owe, M., de Jeu, R., Holmes, T., 2008. Multisensor historical climatology of satellite-derived global land surface moisture. J. Geophys. Res. Earth Surf. 113 (F1). http://dx.doi.org/10.1029/2007JF000769.

Parrens, M., Wigneron, J.-P., Richaume, P., Mialon, A., Al Bitar, A., Fernandez-Moran, R., Al-Yaari, A., Kerr, Y.H., 2016. Global-scale surface roughness effects at L-band as estimated from SMOS observations. Remote Sens. Environ. 181, 122–136.

Patton, J., Hornbuckle, B., 2013. Initial validation of SMOS vegetation optical thickness in Iowa. IEEE Geosci. Remote Sens. Lett. 10 (4):647–651. http://dx.doi.org/10.1109/LGRS.2012.2216498.

Piles, M., McColl, K.A., Entekhabi, D., Das, N., Pablos, M., 2015. Sensitivity of aquarius active and passive measurements temporal covariability to land surface characteristics. IEEE Trans. Geosci. Remote Sens. 53 (8), 4700–4711.

Simard, M., Pinto, N., Fisher, J.B., Baccini, A., 2011. Mapping forest canopy height globally with spaceborne lidar. J. Geophys. Res. Biogeosci. 116 (November):1–12. http://dx.doi.org/10.1029/2011JG001708.

SMAP Algorithm Development Team and Science Team, 2016. Ancillary Data Report on Surface Temperature. Jet Propuls. Lab. Calif. Inst. Technol., JPL, p. D-53064.

Tian, F., Brandt, M., Liu, Y.Y., Rasmussen, K., Fensholt, R., 2016a. Mapping gains and losses in woody vegetation across global tropical drylands. Glob. Chang. Biol. 1–13. http://dx.doi.org/10.1111/gcb.13464.

Tian, F., Brandt, M., Liu, Y.Y., Verger, A., Tagesson, T., Diouf, A.A., Rasmussen, K., Mbow, C., Wang, Y., Fensholt, R., 2016b. Remote sensing of vegetation dynamics in drylands: evaluating vegetation optical depth (VOD) using AVHRR NDVI and in situ green biomass data over West African Sahel. Remote Sens. Environ. 177:265–276. http://dx.doi.org/10.1016/j.rse.2016.02.056.

Ulaby, F.T., Long, D.G., 2014. Microwave Radar and Radiometric Remote Sensing. The Univerity of Michigan Press, Ann Arbor.

Van de Griend, A.A., Owe, M., 1994. Microwave vegetation optical depth and inverse modeling of soil emissivity using nimbus SMMR satellite-observations. Meteorog. Atmos. Phys. 54 (1–4), 225–239.

Van der Schalie, R., Parinussa, R.M., Renzullo, L.J., van Dijk, A.I.J.M., Su, C.-H., de Jeu, R.a.M., 2015. SMOS soil moisture retrievals using the land parameter retrieval model: evaluation over the Murrumbidgee Catchment, southeast Australia. Remote Sens. Environ. 163:70–79. http://dx.doi.org/10.1016/j.rse.2015.03.006.

Vittucci, C., Ferrazzoli, P., Kerr, Y., Richaume, P., Guerriero, L., Rahmoune, R., Vaglio Laurin, G., 2016. SMOS retrieval over forests: exploitation of optical depth and tests of soil moisture estimates. Remote Sens. Environ. 180, 115–127.

Vrieling, A., De Leeuw, J., Said, M.Y., 2013. Length of growing period over africa: variability and trends from 30 years of NDVI time series. Remote Sens. 5 (2):982–1000. http://dx.doi.org/10.3390/rs5020982.

Wigneron, J.-P., Parde, M., Waldteufel, P., Chanzy, A., Kerr, Y., Schmidl, S., Skou, N., 2004. Characterizing the dependence of vegetation model parameters on crop structure, incidence angle, and polarization at L-band. IEEE Trans. Geosci. Remote Sens. 42: 416–425. http://dx.doi.org/10.1109/TGRS.2003.817976.

Wigneron, J.-P., Jackson, T.J., O'Neill, P., Lannoy, De, de Rosnay, P., Walker, J.P., Ferrazzoli, P., Mironov, V., Bircher, S., Grant, J.P., Kurum, M., Schwank, M., Munoz-Sabater, J., Das, N., Royer, A., Al-Yaari, A., Al Bitar, A., Fernandez-Moran, R., Lawrence, H., Mialon, A., Parrens, M., Richaume, P., Delwart, S., Kerr, Y., 2017. Modelling the passive microwave signature from land surfaces: a review of recent results and application to the L-band SMOS and SMAP soil moisture retrieval algorithms. Remote Sens. Environ. 192, 238–262.

Yilmaz, M.T., Crow, W.T., 2014. Evaluation of assumptions in soil moisture triple collocation analysis. J. Hydrometeorol. 15 (3):1293–1302. http://dx.doi.org/10.1175/JHM-D-13-0158.1.